Research Article

Xiaoyan Huang, Xiaohui Zhang*, and Shan Qing

Effect of temperature and nanoparticle size on the interfacial layer thickness of TiO_2–water nanofluids using molecular dynamics

https://doi.org/10.1515/ntrev-2024-0114
received February 28, 2024; accepted October 10, 2024

Abstract: In the design and optimization of nanofluids, it is crucial to investigate and characterize the thermal conductivity enhancement mechanisms and their influencing factors. Although the effect of the "liquid film" on the thermal conductivity of the solid–liquid interface in nanofluids has been extensively studied, most of the research in this area has examined metal–water nanofluids or Ar-based nanofluids. In this work, non-equilibrium molecular dynamics is utilized to explore the mechanism of thermal conductivity enhancement in TiO_2–water nanofluids. It is noted that a distinct interfacial layer is formed within 5 Å from the nanoparticle surface. As the nanoparticle size increases, the number density also increases, resulting in a corresponding increase in the thermal conductivity. Moreover, adding 1% TiO_2 nanoparticles to water leads to an increase in thermal conductivity of 1.5–3%. Notably, the interfacial layer thickness remains relatively constant with the change in temperature. The Materials Studio analysis results indicated that the water molecule will have stable chemisorption on the titanium dioxide surface with an adsorption energy of approximately −0.96 eV. The findings of this study offer new insights and useful information to support the selection of nanomaterials for the preparation of convective systems.

Keywords: nanofluids, interfacial layer thickness, molecular dynamics

*** Corresponding author: Xiaohui Zhang,** Faculty of Metallurgical and Energy Engineering, Kunming University of Science and Technology, Kunming, 650093, China; National Local Joint Engineering Research Center of Energy Saving and Environmental Protection Technology in Metallurgy and Chemical Engineering Industry, Kunming University of Science and Technology, Kunming, 650093, China,
e-mail: xiaohui.zhang@kust.edu.cn, tel: +86 18487319560
Xiaoyan Huang, Shan Qing: Faculty of Metallurgical and Energy Engineering, Kunming University of Science and Technology, Kunming, 650093, China; National Local Joint Engineering Research Center of Energy Saving and Environmental Protection Technology in Metallurgy and Chemical Engineering Industry, Kunming University of Science and Technology, Kunming, 650093, China

Nomenclature

A	cross-sectional area perpendicular to the heat flux direction (m^2)
E	energy (kcal/mol)
EMD	equilibrium molecular dynamics
F	vector sum of all the interaction forces between atoms
k	thermal conductivity (W/m K)
L–J	Lennard–Jones
M–A	Matsui–Akaogi
m	mass of the atom
MS	Materials Studio
N	number of particles
n	number of molecules per unit volume
NEMD	non-equilibrium molecular dynamics
q	heat flux (W/m^2)
RDF	$g(r)$ radial distribution function
r	molecular spacing between particle i and particle j (m)
T	temperature (K)
V	volume of the system (m^3)
v	velocity of the atom (m/s)

Greek symbols

ε	energy constant (eV)
σ	length constant (Å)
$\nabla\varphi$	gradient of the potential function

Subscripts

f	base fluid
i	numbering of atom i

j	numbering of atom j
nf	nanofluids
ads	adsorption

1 Introduction

In various engineering applications, the cooling of high-temperature components in heat exchange systems poses a challenge to the effective utilization of traditional heat transfer media. The emergence of nanofluids [1] provides a new way to address this problem. A nanofluid is a new type of heat transfer medium formed by adding nano-scale metal or non-metal oxide particles to the liquid in a certain way and proportion. In the past two decades, a large block of theoretical investigations [2–6] and experimental studies [7–10] have been presented, dealing with various aspects of nanofluids and exploring the technical mechanism of nanofluids in enhancing heat transfer.

TiO_2 is a non-toxic and corrosion-resistant inorganic compound that is characterized by its low cost and high photocatalysis chemical activity. Due to its stable thermal, physical, and chemical properties, it is widely employed in various engineering applications, including dye-sensitized solar cells, dielectric materials, optical catalysts, gas sensors, and electrochromic devices. Rutile is one of the forms of titanium dioxide in nature, with good light scattering and reflection properties and a high refractive index. Rutile is non-toxic and has a chemical inertness in strong acid or alkali environments. These appealing characteristics make it one of the most stable mechanical materials. It is worth noting that many applications of titanium dioxide are inseparable from water, such as water treatment processes and nanofluids.

Anomalous thermal conductivity enhancement of nanofluids has gained large interest from numerous researchers. The same applies to TiO_2–water nanofluids. In this regard, many researchers have investigated the main factors affecting the thermal conductivity of TiO_2–water nanofluids [11,12], including volume fraction, temperature, size, and shape. It was shown that the nanofluid's thermal conductivity increases with an increase in the nanoparticle's thermal conductivity (types of nanoparticles), particle volume fraction, and system temperature. A summary of the main parameters and results of some experimental research evaluations dealing with the effective thermal conductivity of TiO_2–water nanofluids is presented in Table 1.

The results reported earlier highlight that, under the same conditions, adding TiO_2 nanoparticles can enhance the thermal conductivity of the base solution. This can be demonstrated through experiments. However, heat conduction is a microscopic process that is established under the action of microscopic particle thermal motion, including molecules, atoms, and free electrons. In terms of the enhancement mechanisms of heat transport in nanofluids, four main mechanisms have been widely used and reported in the literature: the Brownian motion of nanoparticles, the liquid layering at the liquid/particle interface, the nature convection of heat transport across nanoparticles, and nanoparticle clustering [16].

In addition, recent studies have demonstrated that the layering of base fluid molecules on the surface of solid particles is one of the major mechanisms to enhance heat transfer in nanofluids [17]. Overall, liquid molecules can form an ordered layer structure as a shell at solid surfaces whose atomic arrangement is more ordered than that of the bulk liquid. This structure is commonly known as the interfacial layer. This concept of interfacial layer was first reported by Choi *et al.*, aiming to better understand the thermal conductivity of nanofluids from a microscale perspective [18]. It is noted here that the thickness of the interfacial layer plays a primary role in heat transfer occurring from the solid to the surrounding liquid [19]. Due to the very large specific surface area of nanoparticles, the interfacial layer plays a major role in the heat transfer process from nanoparticles to the base fluids. Additionally, the upper limit for the particle-layered liquid structure is estimated by assuming that the thermal conductivity of the interfacial liquid layer is the same as that of the solid [16]. However,

Table 1: Some experimental research results of the effective thermal conductivity of TiO_2–water nanofluids

Ref.	Nanofluids	Nanoparticle size (nm)	Temperature (°C)	Volume loading (%)	kn_f/k_f
Saleh *et al.* [11]	A-TiO_2–H_2O	33	15–50	0.05–5	1.02–1.215
Pak and Choi [12]	A-TiO_2–H_2O	27	Room temperature	0.99–4.35	1.034–1.108
Zhang *et al.* [13]	TiO_2–H_2O	40	Room temperature	1.2–2.6	1.036–1.054
Yoo *et al.* [14]	TiO_2–H_2O	25	Room temperature	0.1–1	1.1–1.145
Setia *et al.* [15]	TiO_2–H_2O	—	25	0.5–0.75	1.016–1.025
The current work	r-TiO_2–H_2O	20	30–60	1–2	1.01–1.042

the size of the interfacial layer is too small, and thus, its existence cannot be observed through experiments. To address this, molecular dynamics (MD) is presented as a set of molecular simulation methods that mainly rely on Newtonian mechanics to simulate the motion of molecular systems. With its advantages and simulation capabilities, MD has been implemented in many applications [20–24].

Based on their investigation, Israelachvili [25] reported that the intermolecular forces existing between the particle surface and the liquid are van der Waal's and Coulombic forces. These forces operate over a very short distance, forming the interfacial layer. In another study, Cui *et al.* [17] studied the effects of the nanoparticle shape, size, and material type on the microstructure of the liquid–solid interface absorption layer. Additionally, multiple MD simulations were performed considering Cu–Ar, Au–Ar, Ag–Ar, and Fe–Ar nanofluids. In this regard, several local regions of atom density and energy maldistribution were highlighted in the base fluid due to the addition of the nanoparticles. Moreover, it is noted that the number density of Ar atoms near the nanoparticles is larger than that of the atoms in the base fluid. This may be responsible for the abnormal enhancement in the thermal conductivity of nanofluids. Also, Kang *et al.* [26] examined the relative density of the fluid around nanoparticles. They reported a solid-like liquid layer with a thickness of 0.6 nm on the surface of the nanoparticles. In this layer, the fluid density is about 20–40% higher than the density of the base liquid. In Kang *et al.'s* study [26], the MD simulation results were compared against the results obtained by implementing the conventional effective media theory. It was shown that nanoparticle size has little effect on the enhancement of the thermal conductivity of nanofluids when considering a specific nanoparticle diameter range. In another study, Li *et al.* [27] examined the effect of the molecular layer at the liquid–solid interface on the thermal conductivity of nanofluids using equilibrium MD simulations. In their work, the position of the nanoparticle was monitored, as were the liquid atoms around the nanoparticle. On this basis, a liquid molecular layer with a thickness of approximately 0.5 nm was highlighted. This layer moves with the Brownian motion of the nanoparticle. By analyzing the density distribution of the liquid atoms around the nanoparticle, it is found that with a relatively larger nanoparticle diameter, more Ar atoms will be attracted to form the interfacial layer. Liang and Tsai [28] have demonstrated that the thermal conductivity of the interfacial layer with a thickness of 1 nm is 1.6–2.5 times higher than that of the base fluid.

According to the review of studies and research results presented earlier, it is noted that the base fluid molecules are absorbed to form an ordered and denser nanolayer around nanoparticles. This layered structure, which is similar to a solid-phase shell, encloses the surface of nanoparticles. This is regarded as one of the major reasons behind enhancing the thermal conductivity of nanofluids. However, there are two major gaps in the existing literature. The first issue is the use of argon as the base liquid, which is not practical in engineering applications. Second, when employing water-based nanofluids, metal particles are easily oxidized. On the other hand, rutile TiO_2 nanoparticles are more stable in water-based nanofluids. These particles are less susceptible to deterioration due to oxidation and have a longer service life than metal nanoparticles. Therefore, rutile TiO_2–water nanofluids are selected as the research object in this study. The effect of temperature and nanoparticle size on the interfacial layer thickness of TiO_2–water is studied in this work by combining MD and Materials Studio (MS) analysis.

2 Simulation methodology

2.1 MD model

The MD method is a practical numerical simulation approach based on Newtonian mechanics. It is mainly used to simulate the motion of molecular systems and evaluate the motion state of atoms in the system through numerical simulations. The mass and velocity of atoms are calculated in the simulation system using the following equation [29]:

$$m_i \frac{\mathrm{d}v_i}{\mathrm{d}t} = F_{ij} = \nabla \varphi_{ij}, \tag{1}$$

where m_i and v_i denote the mass and velocity of the atom, respectively. F_{ij} is the vector sum of all the interaction forces between atoms i and j, and $\nabla \varphi_{ij}$ is the gradient of the potential function.

Furthermore, the large-scale atomic/molecular massively parallel simulator (LAMMPS) [30] is a classical MDs code with a focus on material modeling. It has the potential to be applied to solid-state materials (metals, semiconductors), soft matter (biomolecules, polymers), and coarse-grained or mesoscopic systems. LAMMPS can be used to model atoms or, more generally, adopted as a parallel particle simulator at the atomic, meso, or continuum scale. In this work, this simulator is employed to simulate TiO_2–water nanofluids. The simulations are carried out considering a canonical ensemble *NVT* with a certain particle number N, volume V, and temperature T in the system, and a microcanonical ensemble *NVE* with a certain particle

number N, volume V, and energy E in the system. The *NVT* ensemble is used for relaxation and heating, and the *NVE* ensemble is used for data collection and thermal conductivity calculation. In this work, a simulation box with dimensions of 60 Å × 60 Å × 60 Å is used to release water molecules and TiO_2 nanoclusters. The TiO_2 nanocluster from MS is placed in the middle of the cube. Table 2 lists the different structural parameters used in the establishment of the simple point charge (SPC) water model. Additionally, Figure 1 presents the SPC water model and the TiO_2 nanoparticle model. Figure 2 depicts the structure of TiO_2 nanoparticles and water molecules, as well as the respective initial positions in the simulated system.

Moreover, the Matsui–Akaogi (M–A) potential [31] is used to describe the interatomic potentials between Ti–O, Ti–Ti, O–O, and Ti–O_w, and it is represented as follows:

$$U(r_{ij}) = A_{ij} \exp\left(-\frac{r_{ij}}{\rho_{ij}}\right) - \frac{C_{ij}}{r_{ij}^6} + \frac{q_i q_j}{r_{ij}}, \tag{2}$$

where $U(r_{ij})$ denotes the interatomic potential of atoms i and j, and r_{ij} represents the distance between atoms i and j. In this evaluation, the atomic charges of O and Ti are −1.098e and + 2.196e, respectively. The interaction parameters A_{ij}, ρ_{ij}, and C_{ij} used in the M–A potential function are presented in Table 3.

In the SPC water molecular model, the interatomic potentials between O_w–O_w, H–H, and O_w–H are modeled using the Lennard–Jones (L–J) potential [32] and can be represented as follows:

$$U(r_{ij}) = 4\varepsilon_{ij}\left[\left(\frac{\sigma_{ij}}{r_{ij}}\right)^{12} - \left(\frac{\sigma_{ij}}{r_{ij}}\right)^{6}\right]_{r_{ij}\le r_c}, \tag{3}$$

where r_{ij} is the distance between atoms i and j. σ_{ij} and r_{ij} represent the energy and length scales, respectively. r_c is the cutoff distance, selected as 1.0 nm in this investigation for all intermolecular interactions. The interatomic potential between O–O_w is also modeled using the L–J potential [33]. On the other hand, the interaction between hydrogen atoms is neglected because of their respective small masses. On this basis, it is assumed that the interaction between different atoms and H_2O is primarily represented by an interaction between the atoms and oxygen.

Table 2: Structural parameters used in the establishment of the SPC water model

Parameter	Value	Unit
O mass	15.9994	g/mol
H mass	1.008	g/mol
O charge	−0.820	e
H charge	0.410	e
OH bond r	1.0	Å
HOH angle θ	109.47	°
L–J epsilon for O–O (ε_{OO})	0.1553	kcal/mol
L–J sigma for O–O (σ_{OO})	3.166	Å
L–J epsilon for H–H (ε_{HH}), O–H (ε_{OH})	0	kcal/mol
L–J sigma for H–H (σ_{HH}), O–H (σ_{OH})	0	Å
Coulombic cutoff (r_c)	10	Å

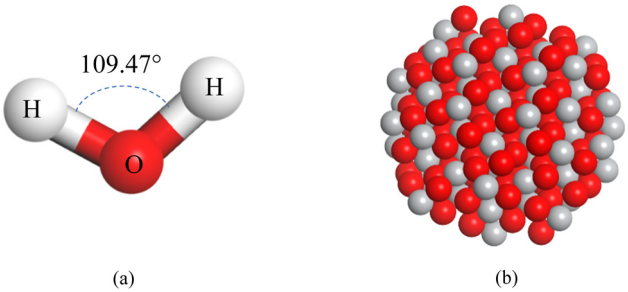

Figure 1: Illustration of the SPC water model. (a) H_2O molecule, and (b) TiO_2 nanocluster.

In the conducted simulations, the time step was set to 1 fs in the non-equilibrium molecular dynamics (NEMD) simulation box, and the long-range Coulomb forces were calculated to reflect the long-range interactions of the molecules. Additionally, periodic boundary conditions were set in the x, y, and z directions of the considered system to reduce the effect of the simulated box size. To eliminate the impact of the initial conditions on the simulation results, the model was completely relaxed under the canonical ensemble (*NVT*) using a Nosé–Hoover thermostat and the microcanonical ensemble (*NVE*) for 100,000 steps. This allows for achieving a stable temperature and energy state. Then, this obtained energy was added to the cold source and heat source regions. The simulation box was run for 70,000 steps under *NVE* to generate a stable temperature gradient and a corresponding heat flow parallel to the y-axis. Finally, the NEMD simulation box was run for another 100,000 steps to calculate the TiO_2–water nanofluid parameters under the *NVE*. Implementing the aforementioned steps, the thermal conductivity k can be calculated using Fourier's thermal conductivity law, combining the following equation:

$$q_y = -k\frac{\mathrm{d}t}{\mathrm{d}y}. \tag{4}$$

Figure 3 shows the influence of the step size on the system temperature, kinetic energy, potential energy, and total energy, considering a temperature range of 303–333 K. It is noted that the system arrives at an equilibrium state within less than 100,000 steps. So, the system is considered

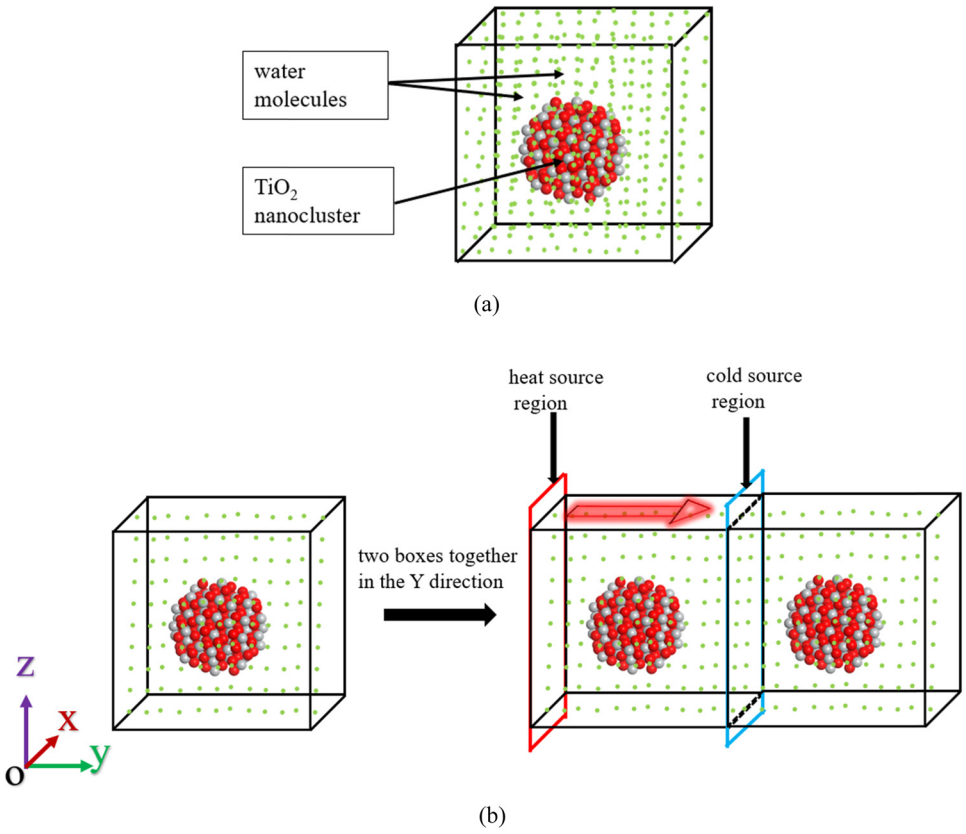

Figure 2: Schematic of the simulation box using NEMD. (a) The initial position of the TiO_2 nanocluster, and (b) simulation box.

Table 3: Interaction parameters for the M–A force field on TiO_2 and water oxygen

i–j	A_{ij} (kcal mol^{-1})	ρ_{ij} (Å)	C_{ij} (kcal mol^{-1} Å^6)
Ti–O	391,049.1	0.194	290.331
Ti–Ti	717,647.4	0.154	121.067
O–O	271,716.3	0.234	696.888
Ti–O_W	28,593.0	0.265	148.000

stable before calculating the thermal conductivity by running 100,000 steps under the *NVT*.

2.2 Adsorption configuration of water molecules on TiO_2(110) surface

2.2.1 Surface energy

As presented in the authors' previous studies dealing with TiO_2–water interfaces, the rutile-(110) surface was cut from bulk rutile with lattice vectors a_0 = b_0 = 4.594 Å and c_0 = 2.959 Å (group name P_{42}/mnm). On this basis, the stability of the surfaces is in the decreasing order 110 > 100 > 101 for rutile [34]. Additionally, the calculation results reported by Ramamoorthy and Vanderbilt have indicated that the (110) surface has the lowest energy due to the low density of dangling bonds on this surface [35]. Based on these findings, it was demonstrated that the rutile-(110) is stable, with considerable experimental data available.

In this study, the computational results were generated using MS. The generalized gradient approximatedensity functional theory using the Perdew–Burke–Ernzerhof exchange–correlation function was employed to describe the electronic exchange and correlation effects. Additionally, the plane-wave-pseudopotential scheme was used with ultrasoft pseudopotentials. First, the rutile-TiO_2 bulk parameters were optimized to establish the (110) surface and evaluate the modeling accuracy. In this regard, different sets of *k*-points and energy cutoff were considered to achieve the aforementioned ends. It is worth noting here that the rutile bulk unit cell is tetragonal with $a = b = 4.594$ Å, $c = 2.959$ Å, internal parameter $x = 0.3048$, and $c/a = 0.644$. Using a 3 × 3 × 3 Monkhorst–Pack mesh corresponding to 25 *k* points in the first Brillouin zone, along with a 680 eV cutoff, the following optimized parameters were obtained: $a = b = 4.60651$ Å, $c = 2.9584$ Å, internal parameter $x = 0.3045$, and $c/a = 0.642$. It was shown that those parameters are

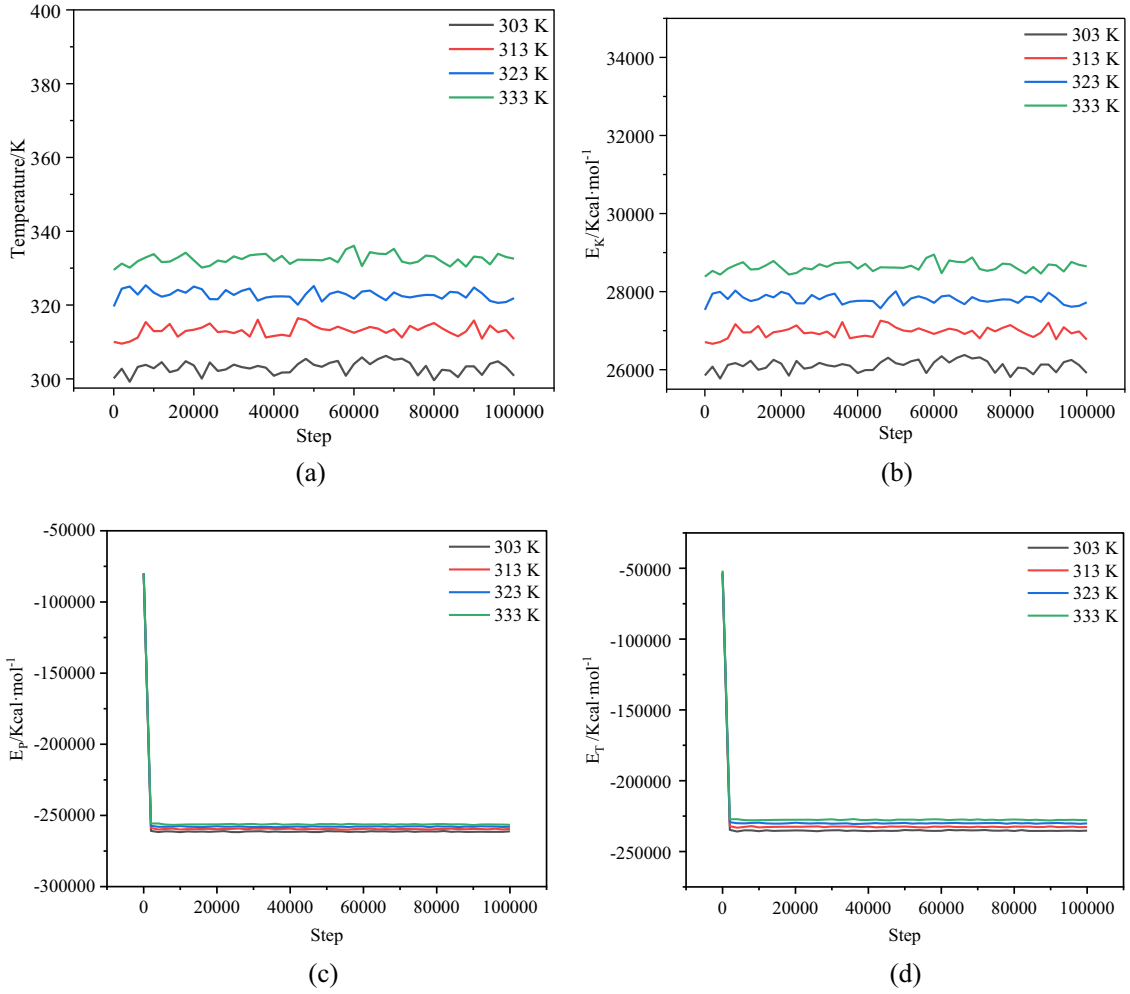

Figure 3: Variation in the system parameters with the step size. (a) Temperature, (b) kinetic energy, (c) potential energy, and (d) total energy.

close to the experimental data reported and are in line with the findings of previous theoretical works, as presented in Table 4. On this basis, the obtained parameters will be used in the subsequent calculations in this study. Furthermore, the rutile-(110) surface was cut for charge compensation to yield a non-polar and dipole free surface [36,37]. It should be noted that all the calculations were performed while neglecting spin polarization and metallization [38]. Also, the positions of all atoms in the supercell were optimized by adopting a conjugate gradient optimization algorithm. The optimized lattice parameters obtained in this work are listed in Table 4.

Furthermore, Figure 4 depicts the atomic structure of the r-TiO_2(110) surface. In the figure, O atoms are shown in red and Ti atoms are shown in gray. O_b denotes a bridging oxygen, O_{3c} represents a three-coordinated surface oxygen, Ti_{5c} is a penta-coordinated surface Ti atom (a lone coordinatively unsaturated site [CUS]), and Ti_{6c} denotes a hexa-coordinated Ti atom. In the bulk, the Ti and O ions are sixfold and threefold coordinated, respectively. At the surface, this coordination is reduced, and the 110 surface is characterized by the presence of rows of twofold-coordinated bridging O ions parallel to the fivefold-coordinated Ti atom, as represented in Figure 4. Additionally, the 110 surface consists of multiple bridging oxygen atoms bonded to a hexa-coordinated Ti atom (Ti_{6c}), as well as a three-coordinated oxygen (O_{3c}) bonded to Ti_{5c} and Ti_{6c} atoms. The surface termination produces CUS, which differ in

Table 4: Optimized rutile lattice parameters (in Å)

Work	*a*	*c*	*x*	*c/a*
Experimental data [39]	4.587	2.954	0.305	0.644
GGA(PAW) [40]	4.649	2.972	0.304	0.640
GGA(PW) [41]	4.651	2.964	0.307	0.637
GGA(LCAO) [41]	4.627	2.981	0.305	0.644
MS	4.594	2.959	0.3048	0.644
The current study	4.60651	2.9584	0.3045	0.642

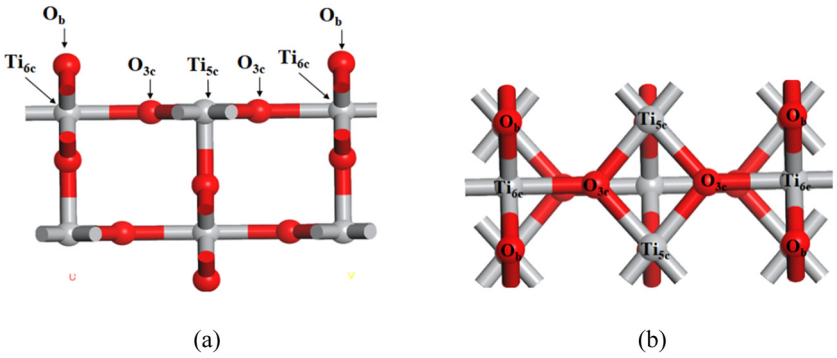

Figure 4: Atomic structure of the r-TiO_2(110) surface. (a) Front view of r-TiO_2 (110), and (b) planform r-TiO_2 (110).

charge from the bulk rutile. From a stoichiometric point of view, the 110 surface would be charge neutral because of the formal ionic charges of +4 and −2 for the Ti and O ions, respectively. From a more covalent point of view, the 110 surface is created by a cleavage of the crystal in which the minimum possible number of bonds has been broken [42].

In addition, it was shown that the surface energy for the unrelaxed slabs, which are the atoms in the bottom layers fixed at the bulk positions, converges very fast with the increase in the slab thickness [42]. In this study, the convergence of the surface energy is tested by MS. Figure 5 presents the test results of the unrelaxed TiO_2(110) surface energy with the increase in slab thickness.

2.2.2 Adsorption configurations

Figure 5 shows that the surface energy experiences strong odd-even oscillations with the increase in the number of layers in the slab, where a very large number of layers is required to obtain well-converged results. Similar oscillations have been reported previously in some studies in the literature [40,42] and are also highlighted in the plots of water adsorption energy. Moreover, Figure 5 highlights that the surface energy becomes more and more stable with more layers. In this regard, for even layer numbers until the tenth layer, the surface energy value is close to that of the second layer. Previous theoretical studies reported a slow convergence of the surface energy and other surface properties with the number of layers in r-TiO_2(110) surfaces [40,42,43]. On the other hand, experimental data is available only for the atomic structure of r-TiO_2(110) in connection with the atomic positions in the first two layers [44]. Thus, to simplify the investigated system and facilitate the calculations, two layers are considered for examination in this study. The rutile-(110) surface was modeled employing a periodic supercell approach with a top value of 0.391. Each supercell contains a rutile (110)-4 × 2 slab in contact with a vacuum layer of thickness of 15 Å.

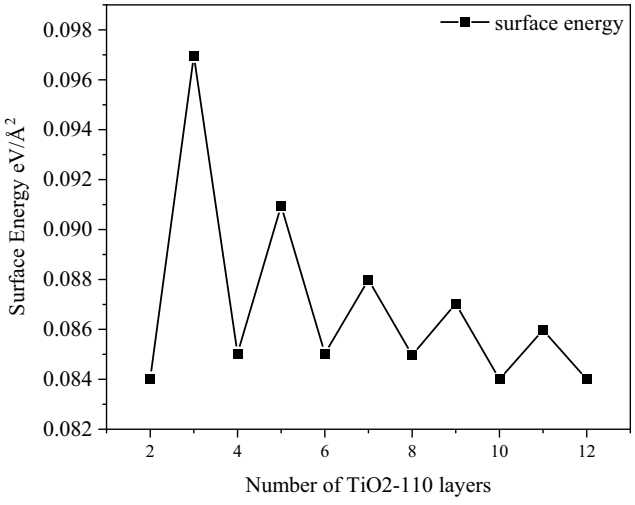

Figure 5: Convergence of the unrelaxed TiO_2(110) surface energy with the slab thickness.

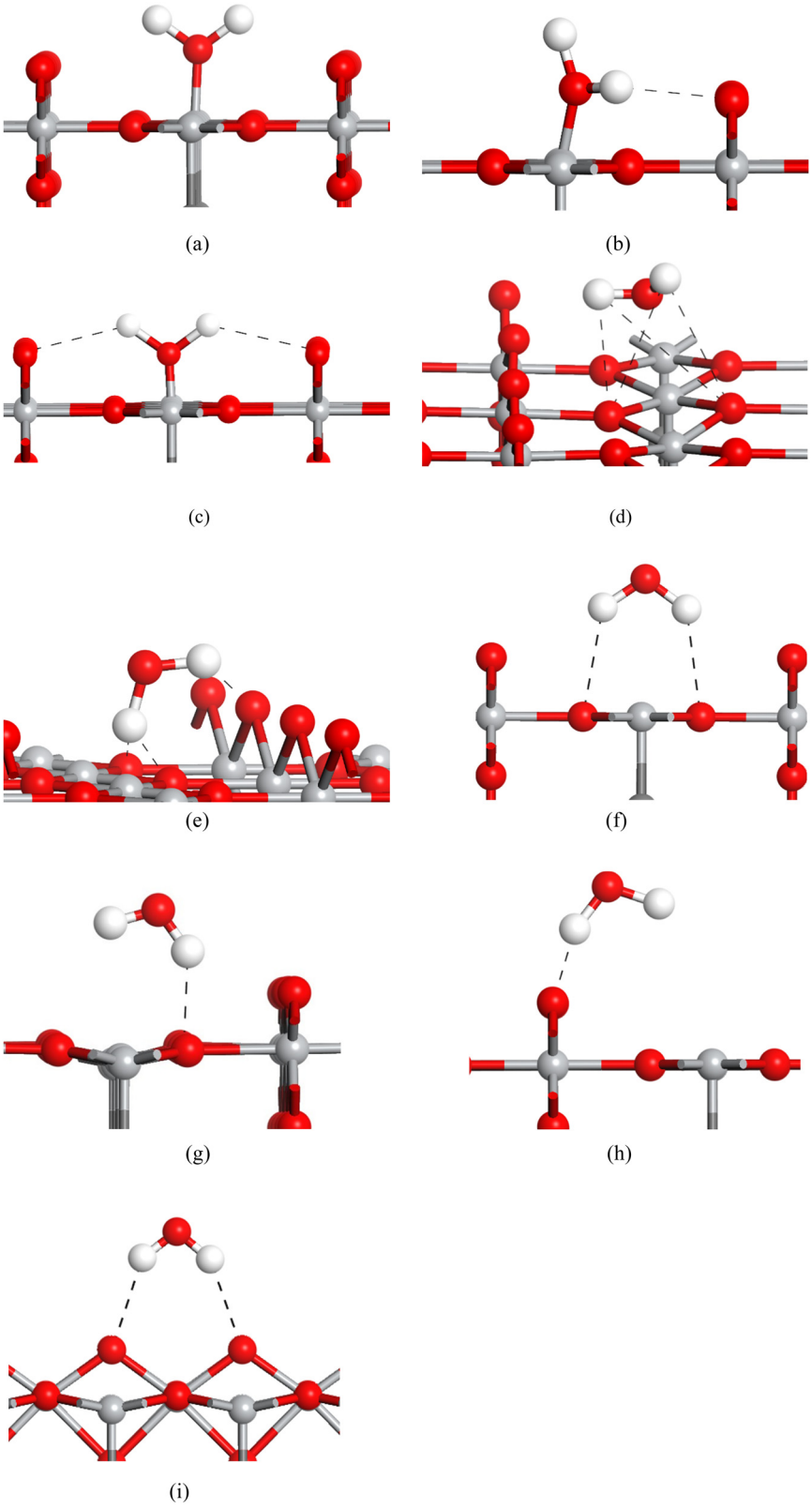

Figure 6: Adsorption configurations of water molecules on the TiO_2(110) surface.

Figure 6 presents the adsorption configurations of a water molecule on the r-TiO_2(110) surface, with the hydrogen bonds represented by black dashed lines.

3 Results and discussion

3.1 Number density

Prior to determining the number density in the TiO_2–water nanofluid systems, a verification of the simulation accuracy and stability was conducted considering a pure water system using the MD method. As shown in Figure 7, through relaxation, water molecules are uniformly distributed, and the temperature gradient is stable in the simulated nucleus. The simulation results of a pure water system are shown in Figure 8(a). Compared to the experimental data reported by Yang and Tao [45], the simulation results have a maximum error of about 2.3%. Thus, it is noted that the simulation results are satisfactory. After validation, the number density distribution of water molecules in the simulation box was computed to evaluate the microscopic mechanism of heat conduction enhancement. The thermal conductivity calculation results of titanium–water nanofluids are presented in Figure 8(b). It is noted that adding 1% titanium dioxide nanoparticles to water results in an increase in thermal conductivity of 1.5–3%. It is worth noting here that the number density is defined as the number of particles per unit volume and can be calculated as follows:

$$n = \frac{N}{V}, \tag{5}$$

where N and V represent the number of water molecules and volume of the calculated region, respectively. n indicates the degree of quantity of water molecules in the studied region. To better characterize the number density at different positions from the surface of the nanoclusters, the distance from the nanoclusters' center to the simulation box was evenly divided into 50 parts along the y-axis. Figure 9(a) presents the number density curves for r = 8 Å (volume fraction, 1%) and r = 10.1 Å (volume fraction, 2%). Also, Figure 9(b) shows the variation in the number density with temperature. The results highlighted that the number density has similar characteristics at different radii. Overall, the calculation results obtained in this work are consistent with those reported by Heyhat [33]. When moving away from the surface of the nanoclusters, the number density tends toward a constant value of 33.3 nm^{-3}. Additionally, two distinct interfacial layers are formed around the central nanosphere with a thickness of about 5 Å. This finding is also similar to the results reported in a previous study in the literature [33]. Furthermore, it is noted that the maximum number density value is linearly related to the nanoparticle size, where the higher the number density, the denser the structure. This is conducive to the heat transfer process. It is shown in Figure 9 that the thickness of the interface layer does not change significantly with the increase in temperature or with the increase in nanoparticle size. These findings are in line with previous research results [46], as presented in Figure 10.

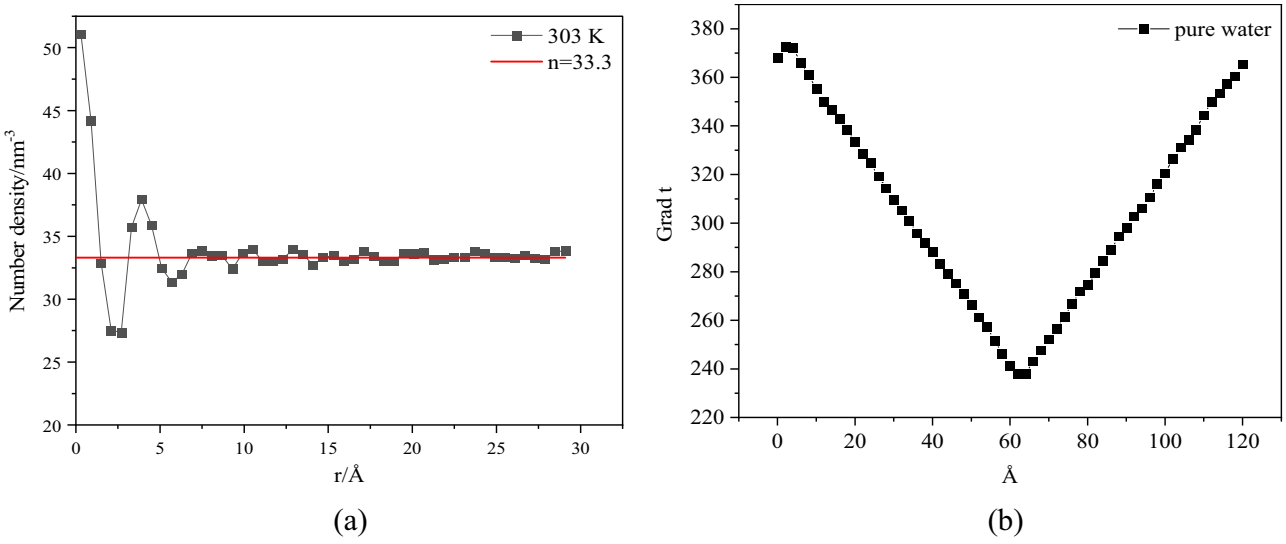

Figure 7: Relaxation results of the simulation system. (a) Number density, and (b) temperature gradient.

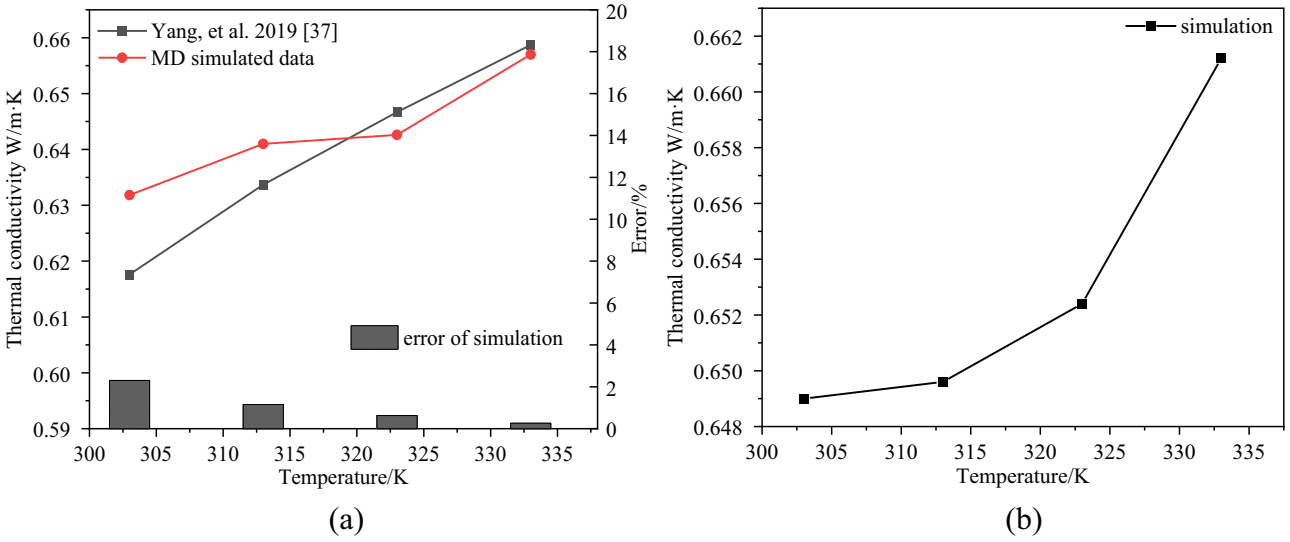

Figure 8: Thermal conductivity calculation results. (a) Pure water, and (b) TiO_2-water nanofluids of 1%.

To fully understand and characterize the interaction between nanoparticle surfaces and water molecules, there is a need for further research to investigate the intrinsic mechanistic aspects. In this case, the radial distribution function (RDF) can be used, which represents the probability of finding a particle at a distance r from the central particle. Figure 11 presents the RDF curves of the rutile TiO_2–water nanofluid. From Figure 11, two distinctive peaks can be noted. The first peak highlights that the interaction between Ti–O_w is closer (approximately 2.3 Å, $g(r)$ = 1.1). The second peak represents the interaction between O–O_w (approximately 3.1 Å, $g(r)$ = 1.3). As shown in the figure, the interaction between O–O_w is stronger than that between Ti–O_w. Meanwhile, the RDF curves reported provide a good explanation and characterization of the behavior and properties of the nanofluid. This includes the trend of "short-range order," "long-range disorder," and finally approaching a constant. This also explains the little variation in the thickness of the nanolayer with the size of the nanoparticles.

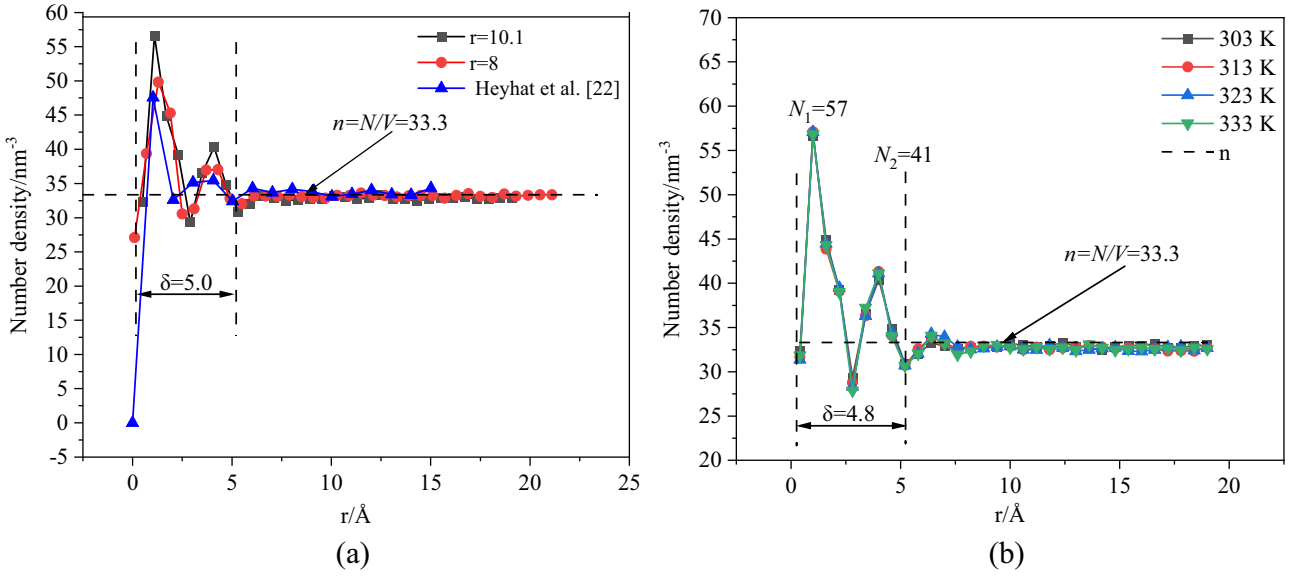

Figure 9: Variations in the number density and atomic surface distance with the nanoparticle size and temperature. (a) Nanoparticle size, and (b) temperature.

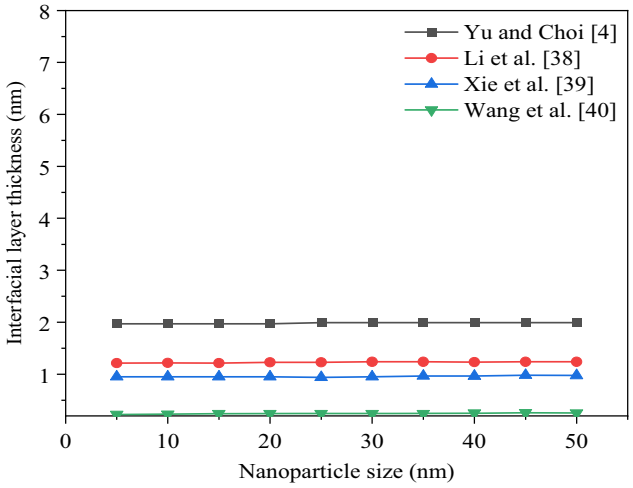

Figure 10: Variations in the interfacial layer thickness with the nanoparticle size.

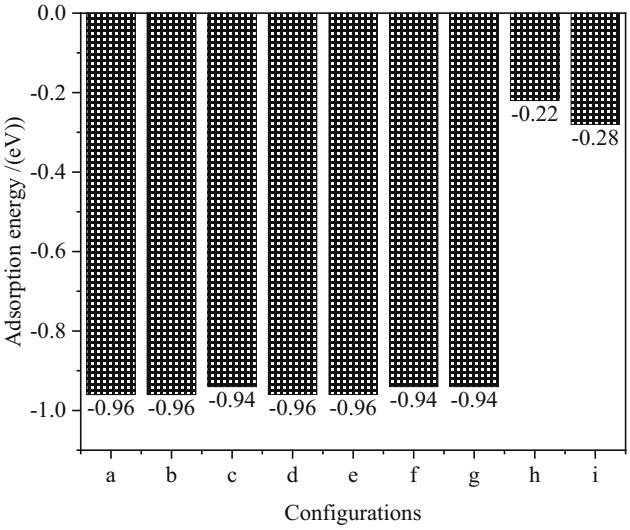

Figure 12: Adsorption energy of the different configurations.

3.2 Adsorption energy

To explain the small variation in the number density with the change in temperature within the studied temperature range (30–60°C), an evaluation of the adsorption types of water molecules on the surface of TiO_2(110) was carried out in this work. As shown in Figure 6, there are a total of nine adsorption configurations formed for water molecules in this study. The adsorption energy E_{ads} can be calculated using equation (6) [47], where all three energies in the equation can be obtained by MS. The calculation results are presented in Figure 12.

$$E_{ads} = E[H_2O + TiO_2(110)] - E[TiO_2(110)] - E[H_2O]. \quad (6)$$

Figure 9 highlights that the number density and thickness of interfacial layers are not consistent with the variation in temperature. Thus, the adsorption characteristics of water molecules on the surface of the TiO_2 nanocluster were examined in this section. As shown in Figure 12, seven of the nine established adsorption configurations (shown in Figure 6(a)–(i)) for water molecules have adsorption energies in the range of [−0.94 and −0.96 eV]. According to the Gibbs free energy concept, negative reaction energy indicates that the reaction can occur freely. In this regard, the more negative the adsorption energy, the more stable the adsorption process. According to the calculation results, all

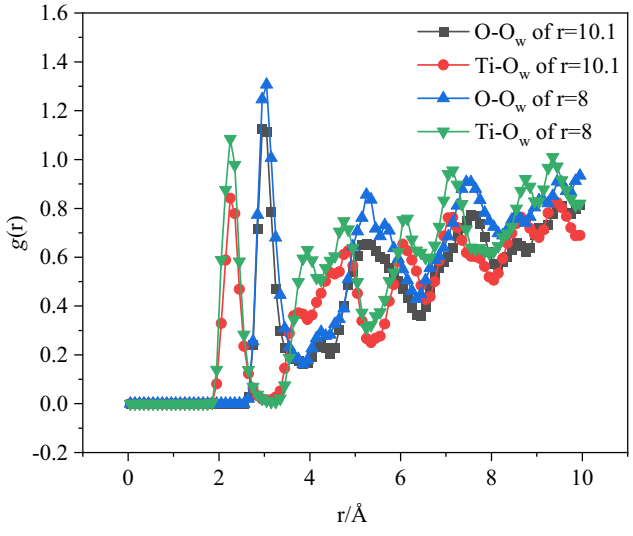

Figure 11: RDF curves of TiO_2–water.

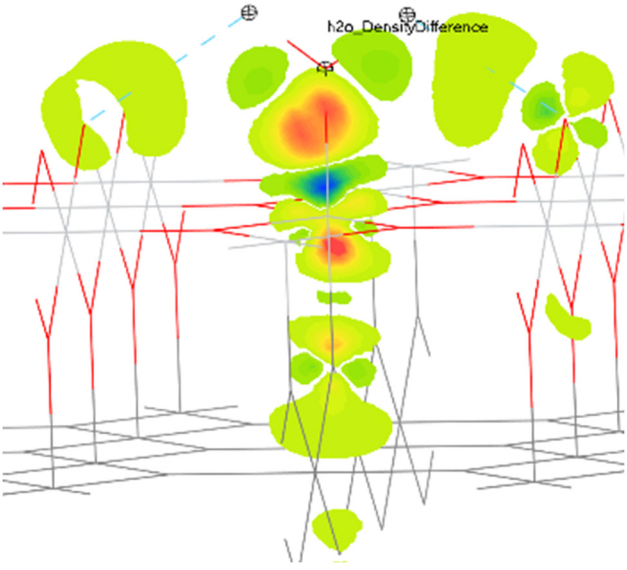

Figure 13: Electron distribution map after adsorbing water molecules.

nine adsorption configurations belong to the chemical adsorption type. Therefore, the adsorption of water molecules on the surface of the TiO_2 nanocluster is found to be stable. Considering the third configuration as an example, Figure 13 shows that the water molecule and surrounding atoms, such as Ti and O atoms, have an overlap and an exchange of electron clouds. On this basis, it is further demonstrated that the two belong to a chemical adsorption type. Overall, compared to physical adsorption, chemical adsorption is considered more stable. In the temperature range of 30–60°C, the number density is found to experience a limited variation with the change in temperature. This is because the temperature is not sufficient to provide the needed energy for water molecules to detach from the TiO_2 surface at this stage.

4 Conclusions

In water-based nanofluids, rutile TiO_2 nanoparticles are generally more stable, less susceptible to deterioration due to oxidation, and have a longer service life than metal nanoparticles. Therefore, rutile TiO_2–water nanofluids were examined and investigated in this study. MD simulations were used to investigate the variation in the interface layer thickness in TiO_2–water nanofluids. An evaluation was carried out to assess the impacts of the nanocluster size and temperature on the interface layer thickness. Additionally, the adsorption energy of the interaction between water and titanium dioxide was reported and analyzed. Based on the findings of this work, the main conclusions are as follows:

The thickness of the interface layer does not increase with the increase in the size of the nanocluster. This is opposite to the variation trend in the number density. This indicates that there is a limited interaction distance between Ti–O_w atoms and O–O_w atoms on a nanocluster surface of less than 5 Å. Meanwhile, the RDF curves provide a good explanation and characterization of the behavior and properties of the nanofluid. This can be described as “short-range order,” “long-range disorder,” and finally approaching a constant.

As the size of the nanocluster increases, the number of surface atoms also increases. This allows for more water molecules to be adsorbed. Therefore, the number density increases with the increase in nanoparticle size. At the same time, the thermal conductivity increases by approximately 1.5–3% at a volume fraction of 1% compared to the case of water alone.

Within the temperature range investigated in this work, it was shown that the thickness of the interface layer varies a little with the change in temperature. The MS analysis carried out demonstrated that water molecules spontaneously undergo chemical adsorption on the TiO_2(110) surface with an adsorption energy of around −0.96 eV. At this stage, it was noted that the considered temperature range cannot provide sufficient energy to allow the water molecules to detach from the surface of TiO_2. This, in turn, results in a small change in the number density with the increase in temperature.

Nanofluids, as a newly developed heat transfer medium in the past two decades, still suffer from major problems that need to be studied in depth. One of the key challenges is the absence of suitable research methods and algorithms for evaluation. For instance, one approach could be the implementation of metaheuristic-based algorithms in the learning of fractional-order memristive neural networks.

Funding information: This work was supported by the National Natural Science Foundation of China (No. 51966005) and the Yunnan Fundamental Research Projects (Nos. 202101AT070120 and 202301AT070469).

Author contributions: All authors have accepted responsibility for the entire content of this manuscript and approved its submission.

Conflict of interest: The authors state no conflict of interest.

Data availability statement: The datasets generated and/or analyzed during the current study are available from the corresponding author on reasonable request.

References

[1] Choi SUS, Eastman JA. Enhancing thermal conductivity of fluids with nanoparticles, Argonne National Lab. (ANL), Argonne, IL (United States), 1995. https://www.osti.gov/biblio/196525.

[2] Noorian H, Toghraie D, Azimian AR. Molecular dynamics simulation of Poiseuille flow in a rough nano channel with checker surface roughnesses geometry. Heat Mass Transf. 2014;50:105–13. doi: 10.1007/s00231-013-1232-x.

[3] Toghraie Semironi D, Azimian AR. Molecular dynamics simulation of liquid–vapor phase equilibrium by using the modified Lennard-Jones potential function. Heat Mass Transf. 2010;46:287–94. doi: 10.1007/s00231-009-0566-x.

[4] Nejatolahi M, Golneshan AA, Kamali R, Sabbaghi S. Nonequilibrium versus equilibrium molecular dynamics for calculating the thermal conductivity of nanofluids. J Therm Anal Calorim. 2021;144:1467–81. doi: 10.1007/s10973-020-09595-x.

[5] Zhang R, Qing S, Zhang X, Luo Z, Liu Y. Enhanced thermal conductivity in Ag–H_2O nanofluids by nanoparticles of different shapes: Insights from molecular dynamics simulation. J Mol Liq. 2023;388:122750. doi: 10.1016/j.molliq.2023.122750.

[6] Li Y, Zhai Y, Xuan Z, Guo W, Wang H. Establishment of thermal conductivity model and analysis of enhancement mechanism in nanofluids: A molecular dynamics study. J Mol Liq. 2022;354:118877. doi: 10.1016/j.molliq.2022.118877.
[7] Hashemzadeh S, Hormozi F. An experimental study on hydraulic and thermal performances of hybrid nanofluids in mini-channel: A new correlation for viscosity of hybrid nanofluids. J Therm Anal Calorim. 2020;140:891–903. doi: 10.1007/s10973-019-08626-6.
[8] Shahul Hameed M, Suresh S, Singh RK. Comparative study of heat transfer and friction characteristics of water-based Alumina–copper and Alumina–CNT hybrid nanofluids in laminar flow through pipes. J Therm Anal Calorim. 2019;136:243–53. doi: 10.1007/s10973-018-7898-z.
[9] Bhattad A, Sarkar J. Hydrothermal performance of plate heat exchanger with an alumina–graphene hybrid nanofluid: experimental study. J Braz Soc Mech Sci Eng. 2020;42:377. doi: 10.1007/s40430-020-02459-3.
[10] Kumar V, Sarkar J. Experimental hydrothermal characteristics of minichannel heat sink using various types of hybrid nanofluids. Adv Powder Technol. 2020;31:621–31. doi: 10.1016/j.apt.2019.11.017.
[11] Saleh R, Putra N, Wibowo RE, Septiadi WN, Prakoso SP. Titanium dioxide nanofluids for heat transfer applications. Exp Therm Fluid Sci. 2014;52:19–29. doi: 10.1016/j.expthermflusci.2013.08.018.
[12] Pak BC, Cho YI. Hydrodynamic and heat transfer study of dispersed fluids with submicron metallic oxide particles. Exp Heat Transf. 1998;11:151–70. doi: 10.1080/08916159808946559.
[13] Zhang X, Gu H, Fujii M. Experimental study on the effective thermal conductivity and thermal diffusivity of nanofluids. Int J Thermophys. 2006;27:569–80. doi: 10.1007/s10765-006-0054-1.
[14] Yoo DH, Hong KS, Yang HS. Study of thermal conductivity of nanofluids for the application of heat transfer fluids. Thermochim Acta. 2007;455:66–9. doi: 10.1016/j.tca.2006.12.006.
[15] Setia H, Gupta R, Wanchoo RK, Tripathi SK, Dharamvir K, Kumar R et al. Thermophysical properties of TiO_2–water based nanofluids. Chandigarh (India): 2011. p. 267–8. doi: 10.1063/1.3653712.
[16] Angayarkanni SA, Philip J. Review on thermal properties of nanofluids: Recent developments. Adv Colloid Interface Sci. 2015;225:146–76. doi: 10.1016/j.cis.2015.08.014.
[17] Cui W, Shen Z, Yang J, Wu S. Molecular dynamics simulation on the microstructure of absorption layer at the liquid–solid interface in nanofluids. Int Commun Heat Mass Transf. 2016;71:75–85. doi: 10.1016/j.icheatmasstransfer.2015.12.023.
[18] Choi SUS, Zhang ZG, Yu W, Lockwood FE, Grulke EA. Anomalous thermal conductivity enhancement in nanotube suspensions. Appl Phys Lett. 2001;79:2252–4. doi: 10.1063/1.1408272.
[19] Yu W, Choi SUS. The role of interfacial layers in the enhanced thermal conductivity of nanofluids: A Renovated Maxwell Model. J Nanoparticle Res. 2003;5:167–71. doi: 10.1023/A:1024438603801.
[20] Wang X, Jing D. Determination of thermal conductivity of interfacial layer in nanofluids by equilibrium molecular dynamics simulation. Int J Heat Mass Transf. 2019;128:199–207. doi: 10.1016/j.ijheatmasstransfer.2018.08.073.
[21] Zarringhalam M, Ahmadi-Danesh-Ashtiani H, Toghraie D, Fazaeli R. Molecular dynamic simulation to study the effects of roughness elements with cone geometry on the boiling flow inside a microchannel. Int J Heat Mass Transf. 2019;141:1–8. doi: 10.1016/j.ijheatmasstransfer.2019.06.064.
[22] Yan SR, Shirani N, Zarringhalam M, Toghraie D, Nguyen Q, Karimipour A. Prediction of boiling flow characteristics in rough and smooth microchannels using molecular dynamics simulation: Investigation the effects of boundary wall temperatures. J Mol Liq. 2020;306:112937. doi: 10.1016/j.molliq.2020.112937.
[23] Jolfaei NA, Hekmatifar M, Piranfar A, Toghraie D, Sabetvand R, Rostami S. Investigation of thermal properties of DNA structure with precise atomic arrangement via equilibrium and non-equilibrium molecular dynamics approaches. Comput Methods Programs Biomed. 2020;185:105169. doi: 10.1016/j.cmpb.2019.105169.
[24] Toghraie D, Hekmatifar M, Salehipour Y, Afrand M. Molecular dynamics simulation of Couette and Poiseuille water-copper nanofluid flows in rough and smooth nanochannels with different roughness configurations. Chem Phys. 2019;527:110505. doi: 10.1016/j.chemphys.2019.110505.
[25] Israelachvili JN. Intermolecular and Surface Forces revised. 3rd edn. New York: Academic; 2011.
[26] Kang H, Zhang Y, Yang M. Molecular dynamics simulation of thermal conductivity of Cu–Ar nanofluid using EAM potential for Cu–Cu interactions. Appl Phys A. 2011;103:1001–8. doi: 10.1007/s00339-011-6379-z.
[27] Li L, Zhang Y, Ma H, Yang M. Molecular dynamics simulation of effect of liquid layering around the nanoparticle on the enhanced thermal conductivity of nanofluids. J Nanopart Res. 2010;12:811–21. doi: 10.1007/s11051-009-9728-5.
[28] Liang Z, Tsai HL. Thermal conductivity of interfacial layers in nanofluids. Phys Rev E. 2011;83:041602. doi: 10.1103/PhysRevE.83.041602.
[29] Wang R, Qian S, Zhang Z. Investigation of the aggregation morphology of nanoparticle on the thermal conductivity of nanofluid by molecular dynamics simulations. Int J Heat Mass Transf. 2018;127:1138–46. doi: 10.1016/j.ijheatmasstransfer.2018.08.117.
[30] LAMMPS Molecular Dynamics Simulator, https://www.lammps.org/.
[31] English NJ, Kavathekar RS, MacElroy JMD. Hydrogen bond dynamical properties of adsorbed liquid water monolayers with various TiO_2 interfaces. Mol Phys. 2012;110:2919–25. doi: 10.1080/00268976.2012.683888.
[32] Chen W, Zhai Y, Guo W, Shen X, Wang H. A molecular dynamic simulation of the influence of linear aggregations on heat flux direction on the thermal conductivity of nanofluids. Powder Technol. 2023;413:118052. doi: 10.1016/j.powtec.2022.118052.
[33] Heyhat MM, Abbasi M, Rajabpour A. Molecular dynamic simulation on the density of titanium dioxide and silver water-based nanofluids using ternary mixture model. J Mol Liq. 2021;333:115966. doi: 10.1016/j.molliq.2021.115966.
[34] Mendive CB, Bredow T, Feldhoff A, Blesa MA, Bahnemann D. Adsorption of oxalate on anatase (100) and rutile (110) surfaces in aqueous systems: experimental results vs. theoretical predictions. Phys Chem Chem Phys. 2009;11:1794. doi: 10.1039/b814608j.
[35] Ramamoorthy M, Vanderbilt D, King-Smith RD. First-principles calculations of the energetics of stoichiometric TiO_2 surfaces. Phys Rev B. 1994;49:16721–27. doi: 10.1103/PhysRevB.49.16721.
[36] Diebold U. The surface science of titanium dioxide. Surf Sci Rep. 2003;48:53–229. doi: 10.1016/S0167-5729(02)00100-0.
[37] Kavathekar RS, Dev P, English NJ, MacElroy JMD. Molecular dynamics study of water in contact with the TiO_2 rutile-110, 100, 101, 001 and anatase-101, 001 surface. Mol Phys. 2011;109:1649–56. doi: 10.1080/00268976.2011.582051.
[38] Cheng H, Selloni A. Hydroxide Ions at the Water/Anatase TiO_2 (101) Interface: Structure and Electronic States from First Principles Molecular Dynamics. Langmuir. 2010;26:11518–25. doi: 10.1021/la100672f.

[39] Muscat J, Swamy V, Harrison NM. First-principles calculations of the phase stability of TiO_2. Phys Rev B. 2002;65:224112. doi: 10.1103/PhysRevB.65.224112.
[40] Perron H, Vandenborre J, Domain C, Drot R, Roques J, Simoni E, et al. Combined investigation of water sorption on TiO_2 rutile (110) single crystal face: XPS vs. periodic DFT. Surf Sci. 2007;601:518–27. doi: 10.1016/j.susc.2006.10.015.
[41] Henderson M. The interaction of water with solid surfaces: fundamental aspects revisited. Surf Sci Rep. 2002;46:1–308. doi: 10.1016/S0167-5729(01)00020-6.
[42] Kowalski PM, Meyer B, Marx D. Composition, structure, and stability of the rutile TiO_2(110) surface: Oxygen depletion, hydroxylation, hydrogen migration, and water adsorption. Phys Rev B. 2009;79:115410. doi: 10.1103/PhysRevB.79.115410.
[43] Wu X, Selloni A, Nayak SK. First principles study of CO oxidation on TiO_2(110): The role of surface oxygen vacancies. J Chem Phys. 2004;120:4512–6. doi: 10.1063/1.1636725.
[44] Charlton G, Howes PB, Nicklin CL, Steadman P, Taylor JSG, Muryn CA, et al. Relaxation of TiO_2(110)-(1 × 1) using surface x-ray diffraction. Phys Rev Lett. 1997;78:495–8. doi: 10.1103/PhysRevLett.78.495.
[45] Yang S, Tao W. Heat transfer. Beijing: Higher Education Press; 2019.
[46] Xie H, Fujii M, Zhang X. Effect of interfacial nanolayer on the effective thermal conductivity of nanoparticle-fluid mixture. Int J Heat Mass Transf. 2005;48:2926–32. doi: 10.1016/j.ijheatmasstransfer.2004.10.040.
[47] Sun, H, Mowbray, DJ, Migani, A, Zhao, J, Petek, H, Rubio, A Comparing quasiparticle H_2O level alignment on anatase and rutile TiO_2. ACS Catal. 2015;5(7):4242–54.